An Investigation of Pore Cracking in Titanium Welds

T. Khaled

Two welded Ti-6Al-4V pressure vessels leaked prematurely in service. The leaks were caused by cracks emanating from weld porosity. The cracks originated during fabrication, with subsequent growth in service leading to the formation of the leak paths. Pore cracking is thought to be caused by a mechanism that involves both sustained-load and cyclic contributions, with the former being the more prominent. It is shown that the tendency for cracking is influenced by pore position and that pore size is not a deciding factor in that regard. The factors that govern pore cracking are discussed, and the possible role of interstitial embrittlement is assessed.

Keywords
crack growth, porosity, titanium alloys, sustained load cracking, welding

1. Introduction

1.1 Problem Statement

A SET of overwrapped spherical pressure vessels is used on the space shuttle to store the helium required to actuate the main engine valves. The maximum operating pressure of these vessels is 4500 psig (31 MPa). A vessel, in its service configuration, consists of a welded 26 in. (0.66 m) diameter Ti-6Al-4V liner, overwrapped with Kevlar-epoxy. The weld, commonly referred to as the girth weld, is at the "equator," whereas the inlet and outlet ports are located at the "north and south poles." A typical duty cycle is such that the vessel is pressurized to 4500 psi (31 MPa) an average of 2 times per flight and held at that pressure for up to several days.

Two pressure vessels of this type, S/N 33 and S/N 35, developed premature leaks in service. The leaks were discovered after nine and ten flights for S/N 33 and S/N 35, respectively. Radiographic inspection revealed cracklike indications associated with weld porosity. No such indications were evident in the radiographs obtained before the vessels were placed in service. It was suspected, therefore, that the leaks in question were caused by these defects. The vessels were removed from service and submitted for a detailed failure analysis. In what follows, weld pores with associated cracks will be referred to as cracked pores.

1.2 Vessel Design

Vessel design is such that liner thickness varies from one location to the other, in order to withstand the anticipated stresses without a weight penalty. Liner thickness at the girth weld is about 0.11 in. (~2.8 mm) and about 0.3 in. (~7.6 mm) at the inlet and outlet ports. Between the girth weld and each of the ports, liner thickness gradually decreases to about 0.068 in. (~1.7 mm). The thin regions are commonly referred to as the membrane. The Kevlar epoxy overwrap has a more or less uniform thickness of about 0.5 in. (~12.7 mm).

T. Khaled, Rockwell International, Space Systems Division, Downey, California.

1.3 Vessel Fabrication

In this type of pressure vessel, the liner is fabricated from two hemispheres, forged from Ti-6Al-4V billets (Mil-T-9047). After forging, the hemispheres are annealed at 1475 °F (802 °C) for 2 h, machined and then penetrant inspected. This is followed by welding the hemispheres by the semiautomatic gas tungsten arc (GTA) method, using Ti-6Al-4V extra-low interstitial (ELI) filler (AMS 4956) and a U-groove joint configuration. Welding is performed in a hard vacuum chamber, under an argon atmosphere. The chamber is evacuated and backfilled with argon several times prior to welding. During welding, the chamber atmosphere is constantly monitored to detect air leaks. A three-pass weld sequence is used, namely, a fusion pass without filler, followed by two filler passes. The welded liner is then annealed at 1175 °F (635 °C) for 2 h, under an argon atmosphere. The next step is to penetrant- and X-ray-inspect the liner. This is followed by proof and leak testing and overwrap application. The overwrapped vessel is then subjected to proof sizing. In this operation, the vessel is pressurized to more than 6000 psig (>41.4 MPa) and held for about 2 min. This high pressure causes the liner membrane to yield, whereas the overwrap deforms elastically. Upon release of pressure, the overwrap attempts to return to its original shape but is resisted by the liner, which has taken a permanent set. The net result of this operation is that the liner membrane is placed under compressive residual stresses, thereby improving the performance of that thinned-down region. The girth weld, on the other hand, does not yield appreciably and, as such, would not get the full benefit of that operation and is left essentially with the residual stresses resulting from welding. Proof sizing is followed by leak testing, at about 5000 psig (~35 MPa). Finally, the vessel is radiographically inspected while pressurized with N_2 at about 700 psig (~5 MPa).

The rigorous testing and inspection to which the liners and then the finished vessels were subjected did not reveal any anomalies in S/N 33 or S/N 35. Only acceptable weld porosity was detected by X-ray inspection. For S/N 33, a total of 89 pores was reported, with pore diameters (sizes) ranging from less than 0.01 to 0.025 in. (<0.25 to 0.64 mm). For S/N 35, a total of 78 pores was reported, with pore sizes ranging from less than 0.01 in. to 0.040 in. (<0.25 to 1.02 mm). No cracks were observed in either vessel. It must be noted, however, that the X-ray inspections performed after welding are double-wall procedures. As such, low energy X-rays and long exposure times

would be required to resolve fine cracks. This would especially be the case after the application of the overwrap.

2. Background

2.1 *Weld Porosity*

Porosity is the result of entrapment of gas bubbles evolving within a solidifying weld pool. To date, several theories have emerged to explain the cause of the culprit gas evolution process. Of these, the most widely accepted is the classical theory, which attributes gas evolution to the rejection of dissolved gases, brought about by a decrease in solubility, as the weld pool cools down (see Ref 1-5). Another theory that is gaining acceptance considers gas evolution to be the result of gaseous products liberated during some chemical reaction, rather than being the result of gas dissolution and solubility changes (see Ref 6-8). The cause of gas evolution aside, the bubbles nucleate at the solid/liquid interfaces and grow by coalescence into larger ones as they rise in the molten pool, under the action of differential flotation rates and strong convective fluid flow. The rising bubbles are eventually trapped by the advancing solidification front(s), leading to the formation of gas porosity. Thus, pore formation involves two steps: (a) nucleation and growth of bubbles and (b) blocking the escape of the rising bubbles. If either step is favorably controlled, weld porosity can be minimized. Welding parameters càn have a profound effect on porosity. Very high welding speeds and chilling lead to high cooling rates, thereby tending to interfere with bubble nucleation and growth. Very slow welding speeds and cooling rates tend to allow the bubbles more time to rise and escape from the surface. These extreme conditions have the general effect of minimizing gas porosity in welds. By contrast, intermediate welding speeds and cooling rates are not effective in controlling either step and, as a result, tend to give rise to more porosity. These trends have been verified by Gorshkov,[5] who also observed that remelting an existing weld joint tends to reduce porosity. The welding process used can also influence porosity. In Gorshkov,[5] electron beam welding, which is performed in vacuum, resulted in more porosity than gas tungsten arc welding, which is performed under argon. This was attributed to the relative ease of bubble formation under vacuum.

The source of gases involved in pore formation can be the environment, the shielding gas, the weld wire, and/or the base metal. In the early days of titanium, many believed that porosity is caused by hydrogen, dissolved in the weld pool. It was also believed that internal hydrogen, contained in the base and filler metals in addition to that picked up from the shielding gas/environment during welding, was the main source of weld porosity. Evans,[6] in a pioneering review, cautioned that hydrogen is a probable, but not the only, cause of porosity in titanium welds. This author pointed out that joint and filler metal cleanliness are also probable causes of porosity. The views advanced by Evans are supported by the results of other studies. For example, Mitchell[7] and D'Andrea[8] concluded that porosity in titanium welds is caused by gas evolving surface films (e.g., oxides, hydrides, and so forth) present on joint surfaces. Furthermore, Mitchell determined that the hydrogen, dissolved

and randomly dispersed throughout the metal, is not the primary cause of porosity. Lawrence et al.,[9] on the other hand, used a light oil film on the weld electrodes as a source to generate porosity in the weld joint. Finally, it has been shown that hydrogen, picked up from the shielding gas during welding, did not cause increased porosity in titanium welds.[10]

In an effort to directly analyze the gases present in titanium weld pores, D'Andrea[8] attempted a novel technique. Mass spectroscopy was used to analyze the spectrum of ionized gases produced by a high frequency arc struck between two electrodes in high vacuum. The electrodes were made of weld specimens containing pores. There was no evidence of any gas release, and D'Andrea concluded that the gases initially involved in pore formation must have diffused away, leaving the pores in a high vacuum state. To date, a clear-cut identification of the gases involved in pore formation has not been achieved. Many authors, however, tend to single out hydrogen as the likely culprit.

2.2 *Pore Cracking in Titanium Welds*

Pore cracking in titanium welds has been the subject of investigation for more than 30 years. Olsen and Gates[11] investigated pore cracking in Ti-5Al-2.5V welds. They noted that pore cracking occurred mainly in restrained sections and that cracking was transverse to the welds. These authors proposed that pore cracking was due to some sort of embrittlement, a reasonable proposition in view of the fact that welding was performed in air. Metallography and microhardness traverses, however, failed to reveal any evidence of that embrittlement. In another study, Walker[12] investigated pore cracking in Ti-6Al-4V welds and concluded that cracking originates at the pores. This author proposed that porosity was due to filler-wire contamination, a proposition that is suggestive of embrittlement. In yet another study, Godfrey et al.[13] examined pore cracking in Ti-3Al-13V-11Cr welds. The authors concluded that alloys with hydrogen content greater than 200 wt ppm were more prone to pore cracking and that the probability of cracking increased with increased porosity. These authors discussed the role of hydrogen in conjunction with pores, embrittlement, and the tendency for cracking, but offered no definitive relationships. In a more recent study, Kennedy and Schulte[14] attempted to explain pore cracking in Ti-6211 welds in terms of oxygen embrittlement. It is clear, therefore, that current thinking tends to associate pore cracking in titanium welds with interstitial (oxygen, hydrogen, and so forth) embrittlement.

Cases of weld pore cracking were also encountered during the development phase of the overwrapped spherical Ti-6Al-4V vessels of the space shuttle. In those cases, proof sizing was suspected to be the cause of pore cracking; a review of these cases may be found elsewhere.[15] Interestingly, weld pore cracking was reported in a nonoverwrapped spherical Ti-6Al-4V vessel.[16] Vessels of this type are intended for lower-pressure service and, because of the absence of an overwrap, no proof sizing is involved. Furthermore, the vessels are welded in the solution treated and aged condition without postweld heat treatments. A detailed investigation concluded that pore cracking is a weld defect.

Table 1 Interstitial analyses results, wt%

	S/N 33			S/N 35		
	Weld metal		Base	Weld metal		Base
Element	With pores	Sound	metal	With pores	Sound	metal
O	0.16	0.17	0.18	0.16	0.15	0.19
H	0.0063	0.0066	0.0077	0.0069	0.0066	0.0071
	(63 ppm)	(66 ppm)	(77 ppm)	(69 ppm)	(66 ppm)	(71 ppm)
N	0.01	0.01	0.01	(a)	(a)	(a)
C	0.021	0.022	0.021	(a)	(a)	(a)

(a) Analysis was not performed.

Table 2 Specification limits

	Composition, wt%	
	Base metal,	Filler wire,
Element	Ti-6Al-4V (Mil-T-9047)	Ti-6Al-4V (ELI) (AMS 4956)
O	0.2 max	0.08 max
H	0.015 max (150 ppm)	0.005 max (50 ppm)

3. Results

3.1 Inspection and Pressure Cycling

3.1.1 S/N 33[15]

After removal from service, S/N 33 was X-ray inspected and then the overwrap was removed. The liner was penetrant- and X-ray inspected. X-ray inspections revealed a multitude of cracked pores. On the film, these are manifested in the form of "tails" transverse to the weld, emanating from and sometimes going through the pores. Penetrant indications were also evident at some of the cracked pore sites. Subsequent leak testing verified the presence of one leak site, through the girth weld, coinciding with the location of both an X-ray indication and a penetrant indication.

To gain some understanding of crack behavior, the liner was pressure cycled. Prior to cycling, however, the liner was heat tinted at 850 °F (454.4 °C) for 20 min in air. The purpose of heat tinting was to mark the extent of the existing cracks that are linked to a free surface and distinguish them from any crack extensions during the cycling test. The cycling conditions were: peak pressure, 1500 psig (10.3 MPa); R, 0.1; frequency, approximately 1 cycle/min; pressurant, water. After 170 cycles, liner failure initiated at the membrane and the test was terminated. Apart from the original leak (leak 1), three additional leaks developed during the cycling test. These additional leaks (leaks 2, 3, and 4) were observed after 60, 100, and 150 cycles, respectively, and their locations also coincided with X-ray indications of cracked pores. It became clear at that point that cracked pores can, and do, cause leaks.

3.1.2 S/N 35 [17]

After removal from service and initial X-ray inspection, it was decided to cycle S/N 35 with the overwrap on. The goal was to allow the leak rate to increase until it became about 10 times the allowable limit of 14 standard cubic in./min (SCIM)

at 2000 psig (229.4 cm^3/min at 13.8 MPa); that is, the target leak rate would be 140 SCIM (2294 cm^3/min) at the stated pressure. This would establish that the leaks would be discovered long before the cracks posed any problem. The cycling conditions were: peak pressure, 4500 psig (30.3 MPa); R, 0.1; pressurant, helium. Dwell times up to 24 h were used at peak pressures in an effort to approximate the long pressurization periods of service conditions. Typically, pressurization required about 20 min, whereas depressurization required another 10 min; that is, a full cycle required about 30 min when no dwell was utilized. The leak rate was constantly monitored to detect any anomalous behavior, indicative of crack instability. It took 96 cycles to achieve the target leak rate, and no instabilities were observed. At that point, the test was discontinued and the overwrap was removed. X-ray inspection of the liner revealed a number of cracked pore indications. The liner was then leak tested. This revealed three leak sites, coinciding with X-ray indications of cracked pores. The leak sites were identified as 1, 2, and 3, for convenience rather than to indicate sequence; because the overwrap was on when the leaks developed, it was not possible to determine the sequence in which they occurred. The liner was then heat tinted as explained earlier.

3.2 Bulk Chemical Analyses

Emission spectrographic analysis was performed on each hemisphere of both S/N 33 and S/N 35. The hemisphere material was verified as Ti-6Al-4V, as specified. The interstitial content of weld regions containing pores was determined and compared to that of sound weld regions and the base metal. The inert gas fusion method was used for oxygen, hydrogen, and nitrogen analyses, whereas the LECO combustion method was used for carbon analysis. Typical results are listed in Table 1. These results show that the interstitial content of the welds is independent of pore presence. The results further show that the oxygen and hydrogen content of the weld metal is lower than that of the base metal, as expected in view of the lower interstitial content of the Ti-6Al-4V ELI filler wire (Table 2). Comparing the data in Tables 1 and 2 reveals that the oxygen and hydrogen content of the weld metal exceeds the maximum limits of the filler-wire specification, an observation that indicates extensive weld metal dilution.

3.3 Metallography and Hardness

Metallurgical sections through the weld were prepared, etched using Kroll's reagent and then examined. In the follow-

ing figures, the letters I and O indicate the inside and outside vessel surfaces, respectively.

The fusion zone (FZ) exhibited a coarse-grained Widmanstättenlike structure (Fig. 1). The base metal (BM) displayed a fine-grained structure, consisting of alpha islands in a transformed beta matrix (Fig. 2). The heat-affected zone (HAZ) displayed a gradual transition between the above extremes (Fig. 3). Microhardness measurements did not reveal any difference between the FZ, HAZ, or BM, which were all in the range HK_{100} 325 to 352. No evidence of alpha case, scale, or any other anomalies was found. The microstructural features and hardness values thus cited were verified in several locations for each vessel.

It was of interest to examine the microstructure near a pore. For this, weld sections containing pores were prepared in the sequence shown in Fig. 4; this sequence was selected to take advantage of the transverse orientation of the cracks, revealed by X-ray inspection. Incremental grinding was used until a pore was intercepted, at which point the section was polished

and then etched using Kroll's reagent. A typical section, through a cracked pore, is shown in Fig. 5, where the crack is seen to be transgranular and transverse to the weld. Microhardness traverses failed to reveal any appreciable hardness changes caused by the presence of that pore. Furthermore, there was no noticeable change in the distribution or type of phases present that could be attributed to or associated with the pore. Examination of several other pores, with and without cracks, confirmed the above findings.

3.4 Fractography

Specimens containing selected pores were notched transverse to the weld and then slowly bent in a vise (Fig. 6) to open up the existing cracks, if any. This notch orientation was selected due to the transverse nature of the cracks, revealed by metallography and X-ray inspection. The resulting fracture surfaces were examined optically and by scanning electron microscopy (SEM). A total of 53 pores, including the 7 leak sites, were examined in that manner. The fracture planes, in all
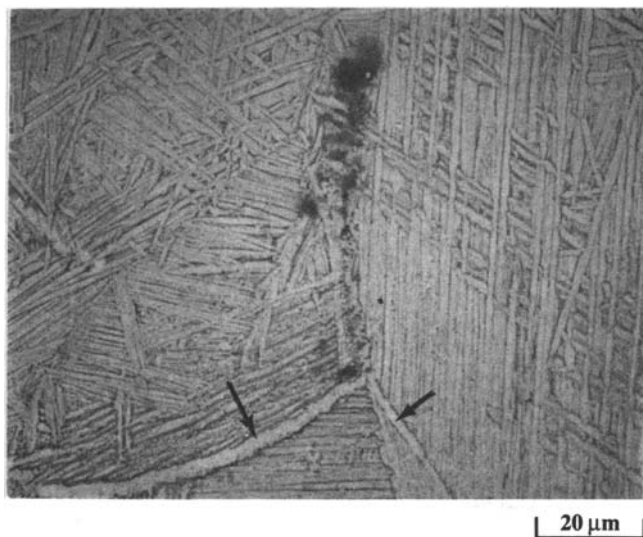

Fig. 1 Fusion-zone microstructure. Widmanstätten structure and alpha (arrows) on prior beta grain boundaries. Shrinkage cavities are also evident. 760×.
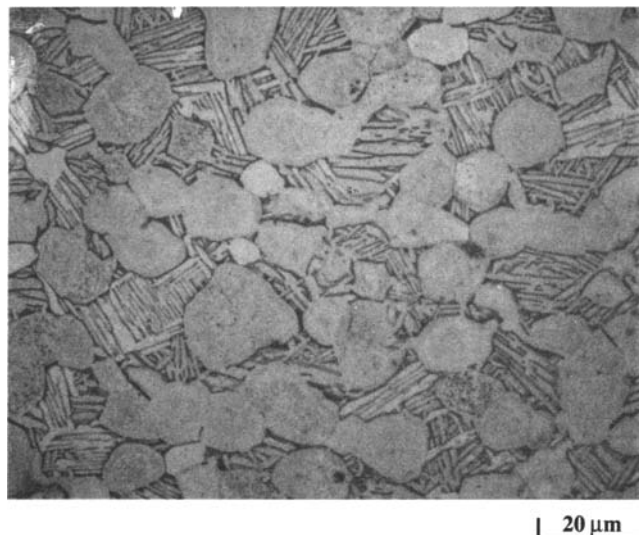

Fig. 2 Base-metal microstructure. Alpha islands (light etching) in a transformed beta matrix. 760×.
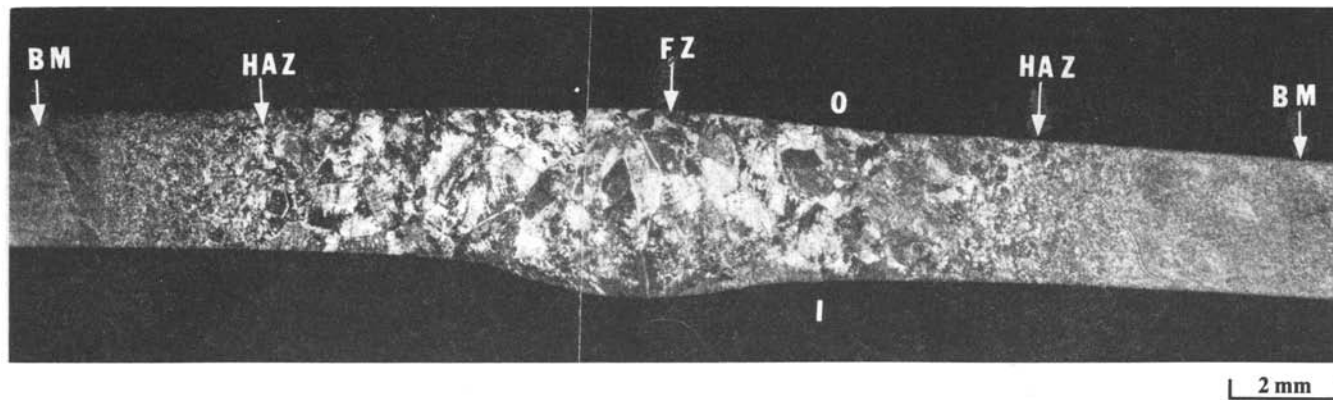

Fig. 3 Metallurgical section through the weld. 7×.

cracked pores, were confirmed to be transverse to the weld with a 10 to 30° off-meridional orientation. In what follows, the letters I, DT, O, and N (depicted on photographs and schematics) will indicate the inside vessel surface, the weld drop-through, the outside vessel surface, and the notches, respectively.

3.4.1 Leak Sites

Leak 1 fracture surface in S/N 33 was examined more extensively than any other site. Figure 7 is an optical micrograph of the fracture surface. The extent of the fracture that existed prior to cycling, hereinafter referred to as the existing fracture, is revealed by the dark color resulting from the heat-tint operation. Crack growth during the cycling test, on the other hand, is manifested in the form of a shiny intermittent band (e.g., arrow) having an average width of 0.004 in. (0.1 mm). It was noted that the existing fracture and the growth band were essentially con-

fined to the fusion zone, on one side of the weld drop-through. Figure 8 is an SEM micrograph of leak 1 fracture surface. The tear ridges (arrows) seen converging to the pore seem to point out that cracking initiated at the pore. Scanning electron microscopy examination of the fracture surface revealed four fracture zones, Z1 through Z4. These zones are schematically identified in Fig. 9. Zones 1 and 2 correspond to the heat-tinted existing fracture, whereas zones 3 and 4 correspond to the cyclic-growth band and the laboratory-induced fracture, respectively. Zone 1 displayed a quasicleavage fracture mode (Fig. 10), which appeared to reflect the underlying Widmanstätten microstructure of Fig. 1. Zone 2, on the other hand, displayed elongated/smeared plateaus (Fig. 11, 12) that contrasted the well-defined angular plateaus of zone 1. The tear ridges, seen throughout zones 1 and 2, generally displayed a dimple rupture fracture mode (Fig. 13). Zone 3, the cyclic-growth zone, was characterized by its small irregular plateaus and rounded-off features (Fig. 14) as well as by the occasional presence of fatigue striations (Fig. 15). The average striation spacing was measured to be about 0.00002 in. (about 500 μm). If it is assumed that each of the 170 cycles produced one striation, the width of the cyclic growth band would be about 0.0034 in. (0.09 mm), in reasonable agreement with the optically determined value of 0.004 in. (0.1 mm). Zone 4, the laboratory-induced zone, displayed a dimple rupture fracture mode (Fig. 16).

The remaining leak-site fracture surfaces of S/N 33 were also examined. Unfortunately, the sites were heat tinted a second time after pressure cycling, prior to opening up the cracks. As a result, fracture zone 3 also became heat tinted, making it impossible to optically distinguish it from the existing fracture. This, in addition to handling damage, made it difficult to identify fracture-zone boundaries as accurately as in the case of leak 1. Scanning electron microscopy examination, however, revealed the same fracture characteristics discussed earlier. Figure 17 shows an optical micrograph of leak 3 fracture surface, whereas Fig. 18 is a schematic of the fracture zones involved;
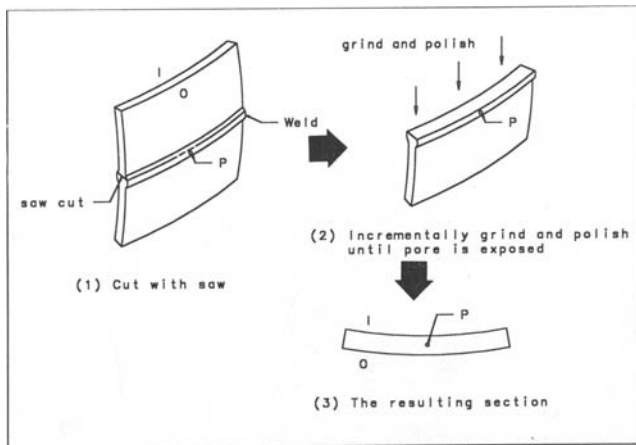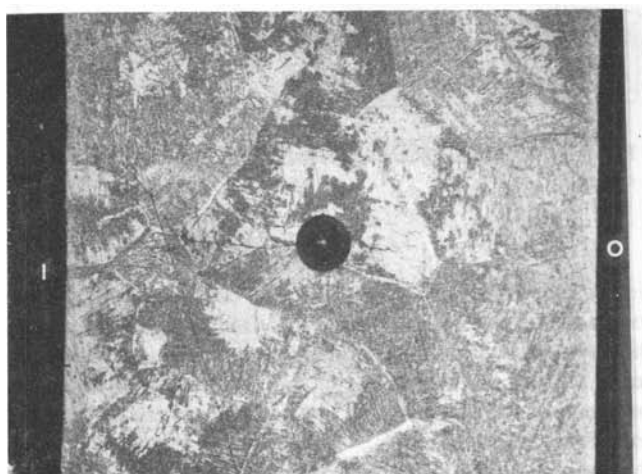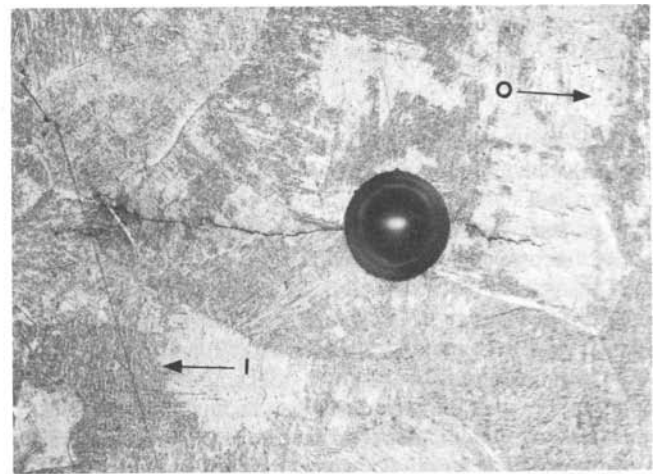

Fig. 4 Metallographic specimen preparation sequence. P designates a pore.

| 0.5 mm |

(a)

| 0.25 mm |

(b)

Fig. 5 A metallurgical section through a cracked pore. (a) 24×. (b) 48×.
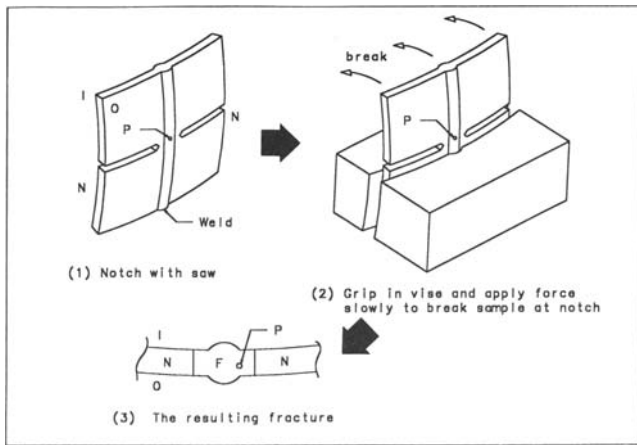
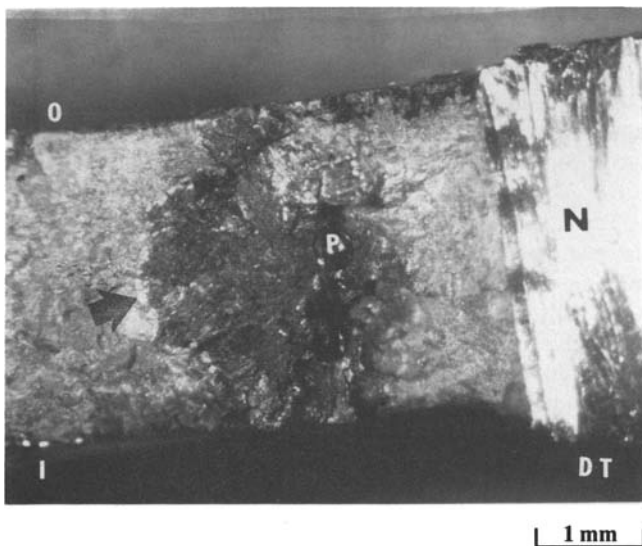Fig. 6 Fractographic specimen preparation. The notches are marked N.

| 1 mm |

Fig. 8 SEM micrograph of leak 1 fracture surface. 15×.

| 1 mm |

Fig. 7 Optical micrograph of leak 1 fracture surface in S/N 33. P marks the location of the pore. 15×.
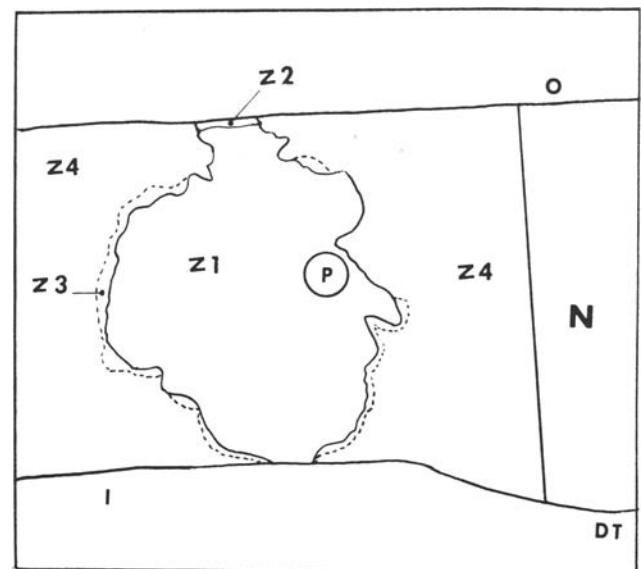
Fig. 9 Four fracture zones, Z1 through Z4, of leak 1. Not to scale.

the regions damaged by handling are marked H in Fig. 18. Interestingly, the crack associated with this leak site escaped X-ray detection.

A cursory examination of the three leak sites of S/N 35 revealed fracture characteristics that are similar to those of S/N 33. The cyclic-growth zone (zone 3), however, averaged about 0.006 in. (0.15 mm), compared to only 0.004 in. (0.1 mm) in S/N 33. Prior to concluding leak-site examination in S/N 35, an effort was made to investigate the effects, if any, of the dwell times used in the cyclic test. In theory, an increase in the dwell time, at a constant maximum pressure, should be accompanied by an increase in striation spacing (or width). Table 3 lists a group of 22 cycles in the sequence they were performed during the pressure-cycling test. Figure 19 shows a region in the cyclic-growth zone of leak 3, where the cycles identified appear to be a close match to those listed in Table 3. It is seen that increasing the dwell time is accompanied by an increase in stria-
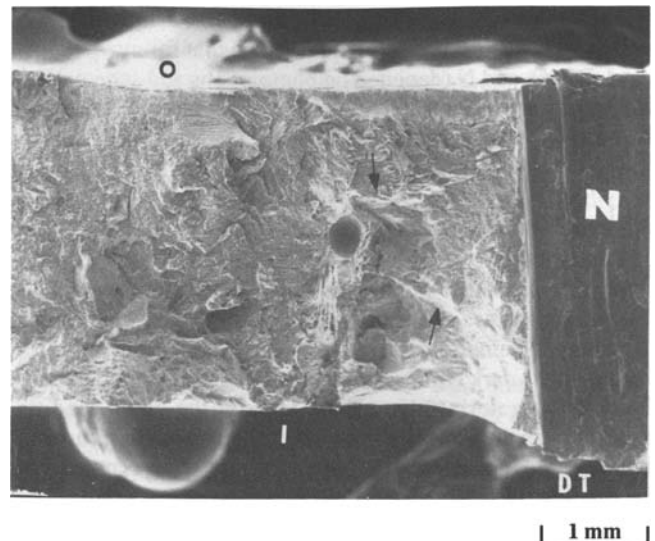
tion width. This aside, Fig. 19 shows that regardless of the length of the dwell time, the resulting steps/striations always display a smooth, rounded-off appearance that is in stark contrast to the angular quasicleavage of zone 1. Arguably, the appearance of the steps would persist if the dwell times were increased to equal those of the service cycles. It became clear at that point that zone 1 quasicleavage could not have been the result of service cycling; zone 2 fracture features would appear to be a closer match to service growth.

To complete leak-site examination, pore sizes were measured using a micrometer-stage microscope. The results are shown in Table 4.
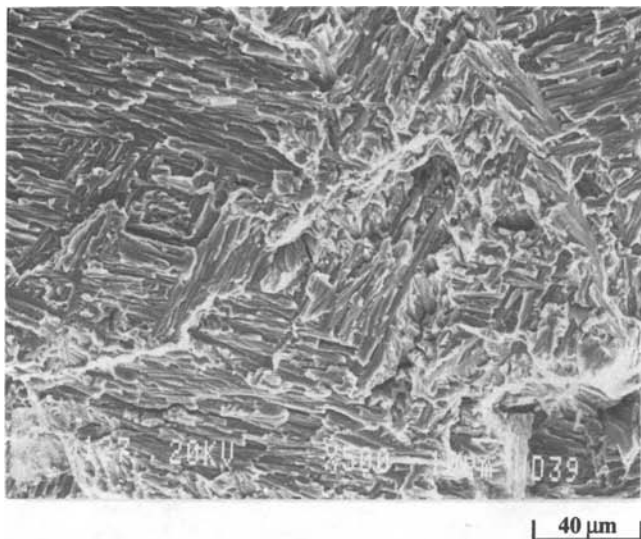
(a)

(b)
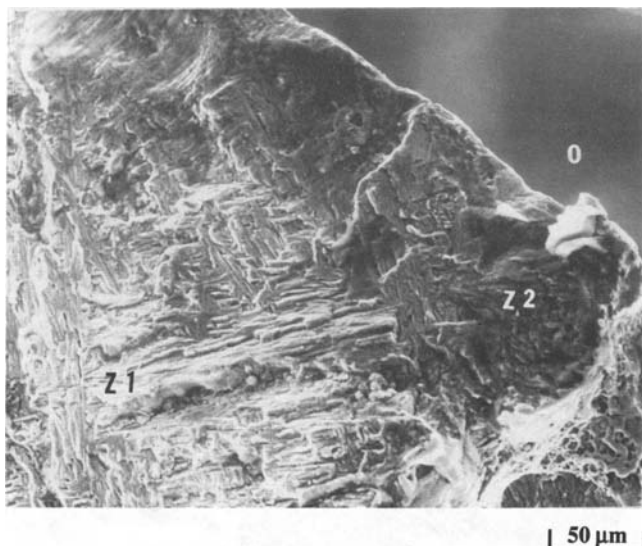
Fig. 10 Zone 1 quasicleavage. (a) 380×. (b) 1520×.

**Fig. 11** Zone 1 to zone 2 transition near the outside vessel surface. 266×.

Fig. 12 The transition of Fig. 11 at higher magnification. 550×.

3.4.2 Other Pore Sites

A group of 46 pore sites were notched and opened up as explained earlier, and the resulting fracture surfaces were examined. A pore was deemed to be uncracked when it was completely surrounded by dimple rupture, with no evidence of quasicleavage or any other fracture mode. Of the 46 sites examined, 17 had uncracked pores, whereas 29 sites were found cracked (Table 5). The fracture features observed were generally similar to those of the leak sites.

Of the 29 cracked pores, 19 had heat-tinted existing fractures, indicating that the cracks were linked to a free surface. By contrast, the remaining 10 sites had unheat-tinted existing

fractures. Figures 20 and 21 show examples of the heat-tinted and unheat-tinted existing fractures; the characteristic tear ridges (arrows) are evident in Fig. 21. The fact that unheat-tinted existing fractures were observed indicates conclusively that cracking initiates within the welds, rather than at the free surfaces; otherwise these fractures would be heat tinted. The tear ridges, seen converging to the pores pinpoint those pores as the initiation sites. The existing fractures associated with pores near the weld face (e.g., Fig. 20a), regardless of pore size, were noticeably small and, as such, are not thought to represent potential leak sites. By contrast, the existing fractures associated with larger pores that are farther from the weld face are generally larger in size (Fig. 21); the leak sites belonged to this category. It was noticed that all existing fractures, large or small, were essentially confined to the fusion zone, on one side of the weld drop-through. In general, the smaller existing fractures (e.g., Fig. 20a) escaped X-ray detection.
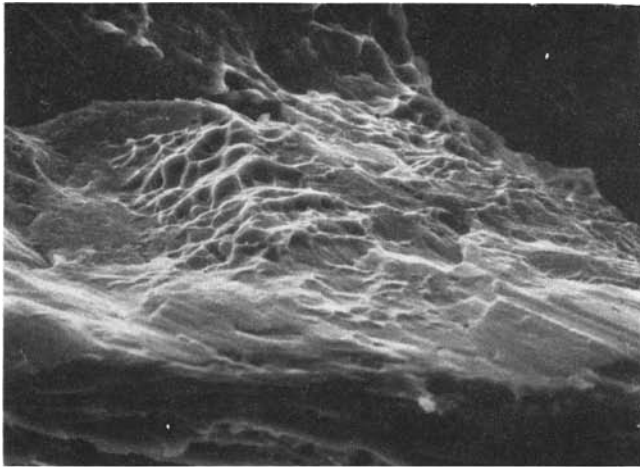
(a)
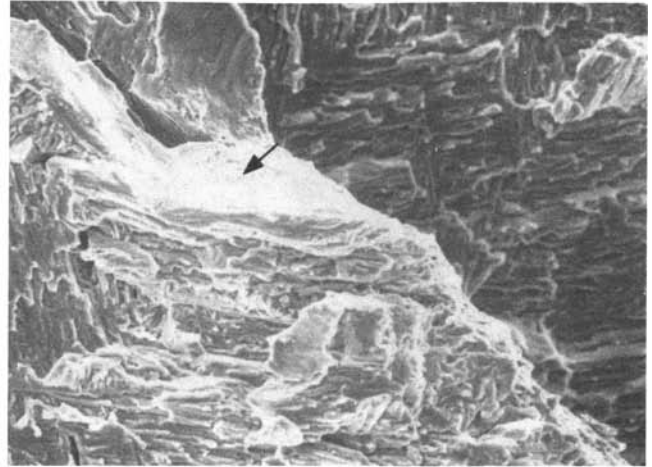
(b)

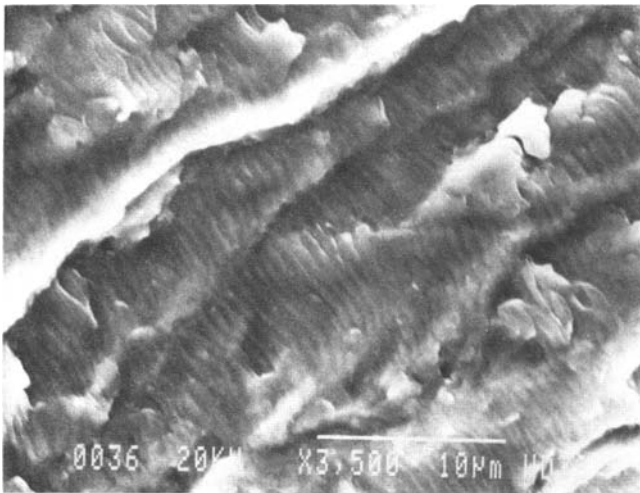**Fig. 13** Tear ridges. (a) Region marked by arrow shown in (b). 307×. (b) Dimple rupture. 1245×.
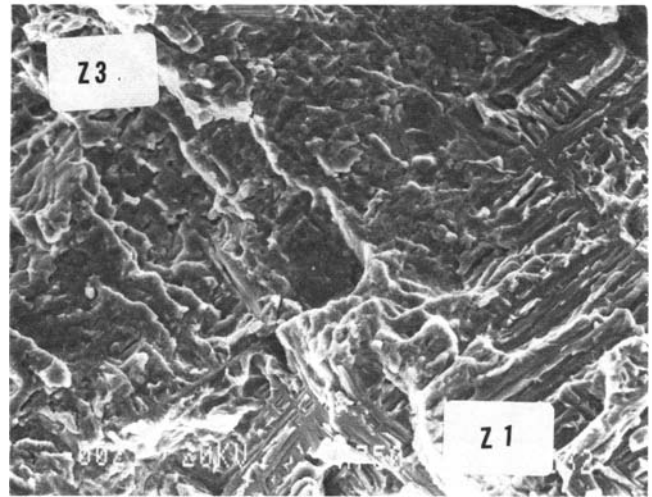

Fig. 14 A typical zone 1 to zone 3 transition. 570×.

Fig. 15 Fatigue striations. 2660×.

Table 3 Dwell times, S/N 35

	Pressure cycle No.							
	75	76	77	78	79-87	88	89-95	96(a)
Maximum pressure, psig (MPa)	4500 (31)	4500 (31)	4500 (31)	4500 (31)	4500 (31)	4500 (31)	4500 (31)	1000-4500 (608-631)
Dwell period, min	1440 (24 h)	16	0	26	0	45	0	>90

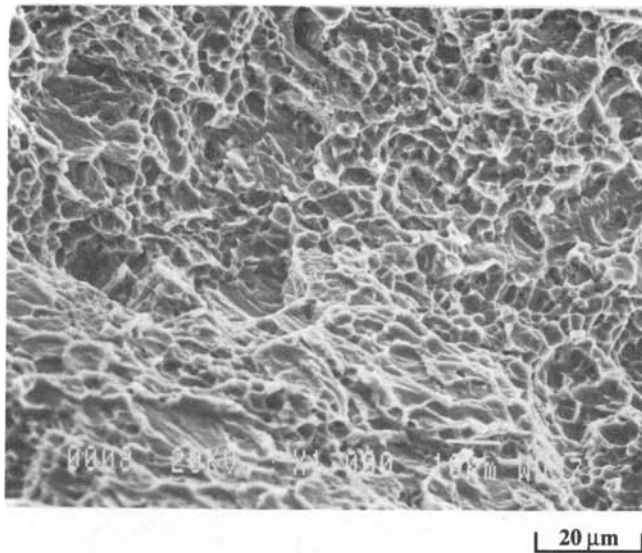(a) This cycle was a survey of leak rate dependence on presssure.
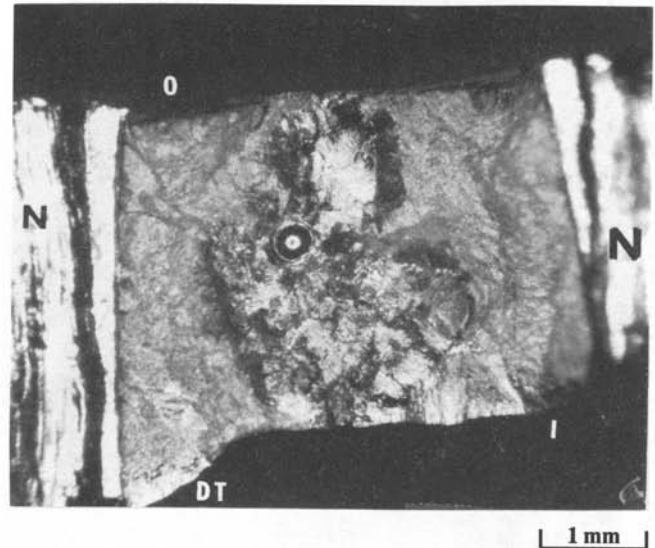
Fig. 16 Dimple rupture in zone 4. 760×.

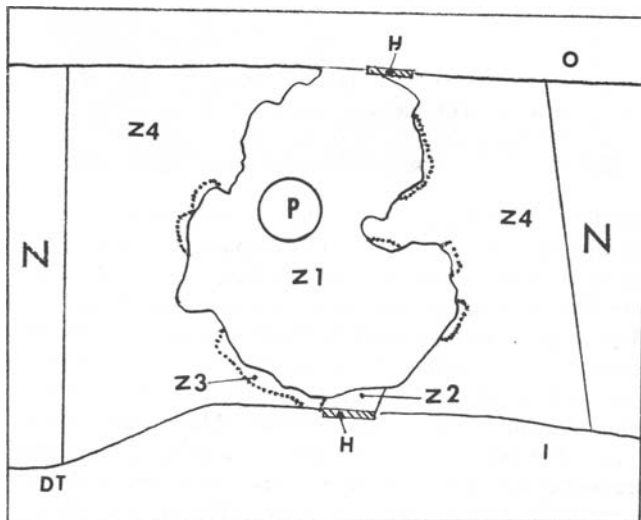Fig. 17 Optical micrograph of leak 3 fracture surface in S/N 33. 15×.

Fig. 18 Fracture zones, Z1 through Z4, of leak 3. Not to scale.

Fig. 19 A portion of the cyclic-growth zone (Z3) of leak site 3, S/N 35. The numbers identify the specific test cycles (Table 4). The laboratory-induced zone (Z4) is to the lower right. 1575×.

Pores as small as 0.01 in. (0.25 mm) in diameter were found to be cracked, whereas pores as large as 0.02 in. (0.50 mm) in diameter were found uncracked. A breakdown of the cracked and uncracked pore sizes (diameters) is presented in Fig. 22. It became clear at that point that cracking is not governed by pore sizes. Godfrey et al.[13] made a similar observation in an earlier study.

The unheat-tinted pore surfaces displayed a shiny, polished appearance. This suggests that the gases, initially responsible for pore formation, were either neutral or reducing in nature.

3.5 Residual Gas and Auger Analyses

Weld and base metal specimens were fractured in a high vacuum Auger microscope, equipped with a residual gas ana-

lyzer.[15] The system typically operates at 10^{-9} torr (1.33×10^{-11} Pa) or better. The gases released upon fracture were analyzed by residual gas analysis (RGA). In weld metal specimens, where fracture intercepted a pore, Auger spectroscopy was used to analyze pore surfaces and the nearby weld fracture surface.

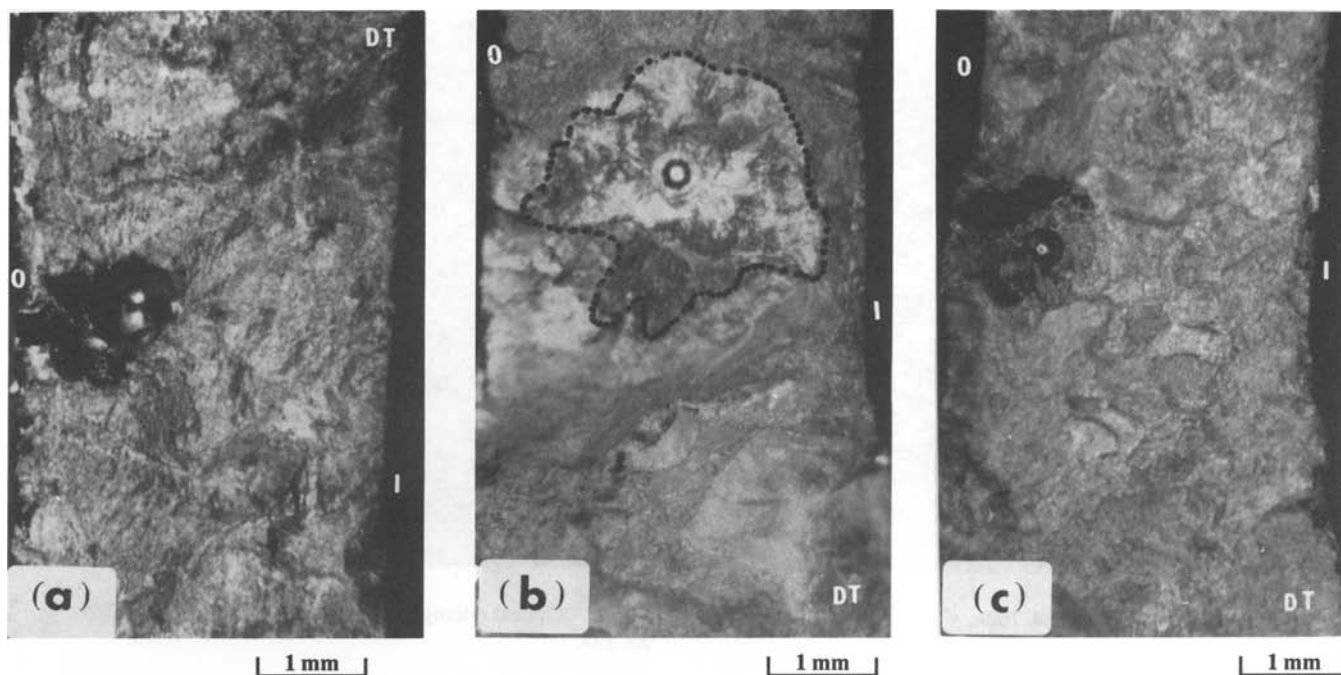**Fig. 20** Optical micrographs of cracked pore fracture surfaces. (a) Pore diameter, 0.025 in. (0.64 mm). Heat-tinted fracture. (b) Pore diameter, 0.015 in. (0.38 mm). Unheat-tinted fracture. Zone 1 boundaries outlined for clarity. (c) Pore diameter, 0.013 in. (0.33 mm). Heat-tinted fracture. All at 15×.

Table 4   Leak-site pore sizes

S/N	Leak site	Pore diameter, in. (mm)
33	1	0.017 (0.43)
	2	0.018 (0.46)
	3	0.018 (0.46)
	4	0.020 (0.50)
35	1	0.020 (0.50)

Residual gas analysis revealed that the most pronounced event, upon specimen fracture, was a release of hydrogen regardless of whether this fracture was through a sound weld, a pore in the weld, or the base metal (Table 6). Furthermore, the amount of hydrogen released upon weld metal fracture was not influenced by pore presence. In other words, no positive association could be made between the presence of pores and hydrogen or, for that matter, any other gaseous species. It was suspected that the pores analyzed were cracked or otherwise linked to a free surface, thereby providing a direct escape path to these gases. Careful examination, however, revealed that this was not the case. It appears, therefore, that the gases initially involved in pore formation must have diffused away from the pores into the weld metal. D'Andrea[8] made a similar observation in an earlier study.

Typical Auger analyses of a pore surface and the surrounding weld metal fracture are shown in Table 7. It must be noted here that Auger spectrometry cannot detect hydrogen. Further-

more, this type of analysis is intended for comparison purposes only, rather than to infer absolute compositions. With these facts in mind, an evaluation of the data shown in Table 7 is possible. The weld metal analysis reflects the basic Ti-6Al-4V composition of the base metal and filler wire. By comparison, the pore surface appears to be covered by some titanium-sulfur layer that is devoid of aluminum and vanadium. This layer has a high potassium content and moderate chlorine and carbon content. The fairly high oxygen content detected on both the pore surface and weld fracture is believed to be largely due to gas reactions in the Auger system. Pore surface analyses, therefore, seem to indicate that the machining oils, the cleaning solutions, and possibly also the gloves (high sulfur) used in fabrication were all culprits in pore formation. These substances would normally be present as contaminants on joint and filler wire surfaces. Several other authors[5-9,18] have made similar observations.

4. Discussion

4.1 Fracture Mode and Fracture Mechanism

Fractographic analyses indicate that pores are the crack-initiation sites. Furthermore, upon discovering the leaks, X-ray inspection revealed a multitude of cracked pores. However, vessel fabrication records show that X-ray inspection after both welding and proof sizing did not reveal any cracks or cracklike indications at the pores. It is clear that some time-dependent mechanism, or combination of mechanisms, is responsible for
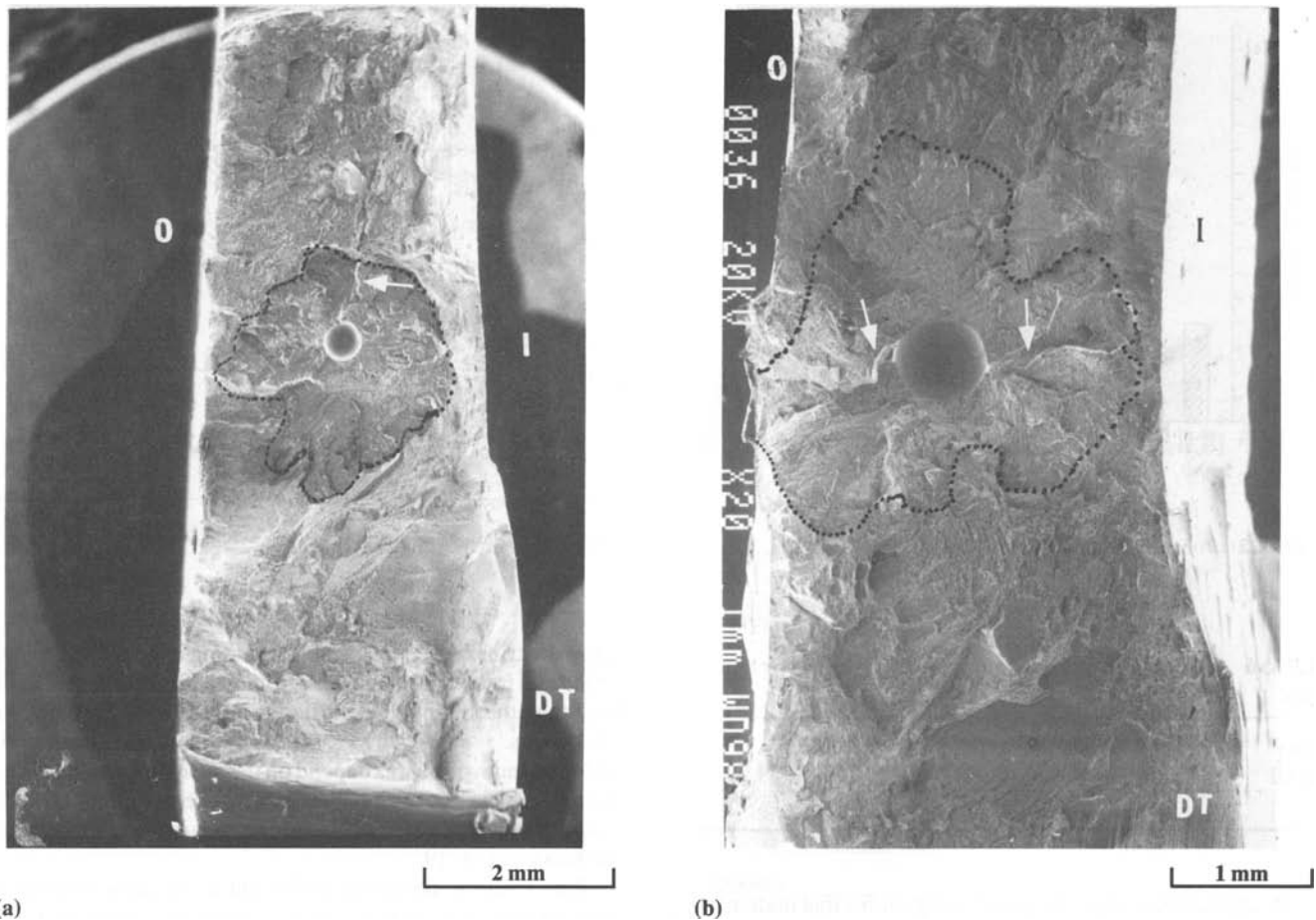
Fig. 21 SEM micrographs of cracked pore fracture surfaces. (a) Pore diameter, 0.015 in. (0.38 mm). Unheat-tinted fracture. Zone 1 boundary outlined for clarity. 13×. (b) Pore diameter, 0.025 in. (0.64 mm). Heat-tinted fracture (not evident in SEM). Zone 1 boundaries outlined for clarity. 20×.

Table 5   Pore-site statistics

| | Cracked pores | | Uncracked | |
S/N	Heat tinted	Unheat tinted	pores	Totals
33	7	7	13	27
35	12	3	4	19

crack initiation at the pores and for the subsequent crack propagation leading to the formation of the observed leaks. In what follows, an effort will be made to shed some light on potential time-dependent mechanisms.

In the development phase of the space shuttle's overwrapped spherical vessels, two weld-failure cases were reported after proof sizing. In one case, a pore was involved, and the fracture surface displayed a quasicleavage mode that is similar to that reported here. In the other case, the same type of quasicleavage was observed even though the weld region that failed contained no pores. The fact that the failures were discovered after the proof-sizing operation led to the conclusion that pore cracking occurs during this operation, if time and

pressure are not properly controlled.[15] In this scenario, it is assumed that the high biaxial stresses, resulting from proof sizing, would lead to local overload and fracture by a quasicleavage mode. This would especially be the case where a pore is present, because the stresses at that location would be more than doubled by the stress concentration factor associated with that pore.[19] Experimental work, however, does not bear out this assumption. It has been shown, using cruciform specimen configurations, that biaxial overload failures in titanium alloys and their welds occur by dimple rupture.[20-22] Pressure-vessel burst tests also show dimple rupture as the biaxial overload fracture mode.[23] Furthermore, weld pore cracking and the attendant quasicleavage have been observed in other tita-
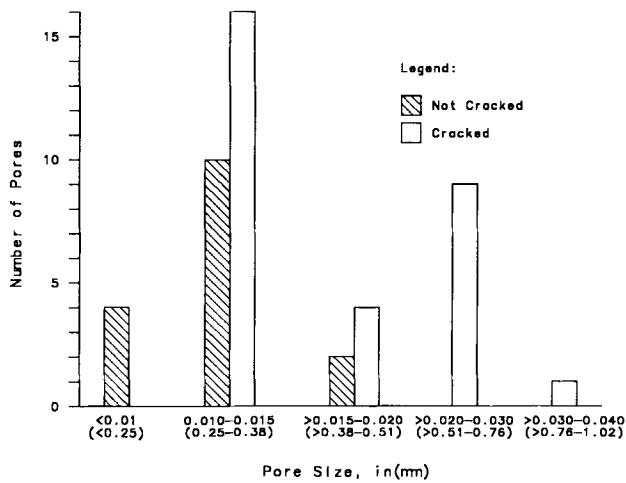
Fig. 22   Pore size (diameter) statistics.

Fig. 23   Pore positions.

Table 6   Typical residual gas analysis amplitudes for hydrogen

Base metal	Sound weld	Pore in weld
103	168	150

nium applications where no proof sizing, or for that matter, any other high-stress operation, was used.[14-16] It appears, therefore, that proof sizing could not be the root cause of weld pore cracking. Noting that, in the two cases just cited, pore cracking was observed before the components were placed in service, residual welding stresses emerge as a likely contributor to pore cracking. The process of cracking under the action of residual stresses is a form of sustained-load cracking (SLC), a failure mechanism to which titanium alloys are known to be susceptible (see Ref 24-26). The confined nature of the fractures observed in cracked pores seems to suggest a decreasing stress field, typical of residual stresses.

It has been shown that residual-stress levels around 30,000 psi (207 MPa) exist at the girth weld of a 0.035-in. (0.9-mm) thick Ti-6Al-4V spherical vessel.[16] Considering that these stresses are doubled by the presence of a pore,[19] the acting stress would be 60,000 psi (414 MPa), which translates to about 40% of the ultimate strength. Higher levels of residual stresses would be expected when using thicker materials,[11] such as those used to fabricate the vessels at hand. Residual stresses of such magnitude are believed to be sufficient for the onset of SLC. The subsequent annealing at 1175 °F (635 °C) for 2 h and proof sizing are not expected to significantly alter the magnitude or distribution of residual stresses within the weld.

Sustained loading and SLC are not peculiar to residual stresses. In fact, the fabrication and service histories of the vessels in question comprises several discrete operations, where the vessel is pressurized to some high pressure and held at that pressure for periods ranging from a few minutes to several days before the pressure is reduced to lower levels. This loading re-
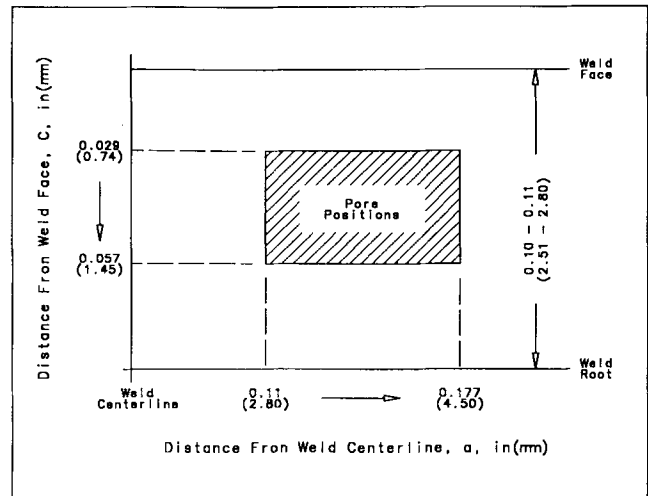
gime describes discrete sustained-loading events that are preceded and followed by periods at lower loads (pressures). In the literature, this regime is identified as fatigue with dwell times at peak loads.[27-31] For the vessel case at hand, the dwell times and maximum pressures depend on the event in question (proof sizing, service cycling, and so forth). The net effect of using longer dwell times is to cause more crack extension per cycle, as shown in Fig. 19.

Pore fracture, therefore, is thought to be caused by dwell-time fatigue, a mechanism that involves both sustained-load and cyclic contributions. The sustained-load contributions, however, appear to be more prominent. Unfortunately, sustained-load and residual-stress implications are seldom, if ever, considered in design analyses.

4.2   Effects of Pore Size and Position

The stress-concentration factor (K_t) associated with a spherical cavity (e.g., a pore) in a semi-infinite solid has been calculated.[19] In that work, K_t is expressed in terms of r/c ratio, where r and c, respectively, are the pore radius (size) and distance from the free surface. Accordingly, pores that are large in size (large r's) and/or close to the free surface (small c's) would have higher K_t values and, as such, should be more likely to crack. The results of the present work, however, indicate that cracking is not governed by pore size. It was suspected, therefore, that the cracking tendency might be influenced by pore position within the fusion zone.

To explore the effect of pore position, a micrometer-stage microscope was used to measure pore coordinates (c) and (a); (c) being the distance between the pore center and weld face and (a) being the distance between pore center and weld centerline. All 53 pores examined in this work existed in a narrow band, close to the weld face (Fig. 23). However, it was recognized that pore position is, at least in part, a function of fusion-zone geometry at that location. It was further recognized that this geometry varies somewhat from vessel to vessel and from location to location, around the girth weld of a given vessel. As a result, the pores were segregated in groups, according to their
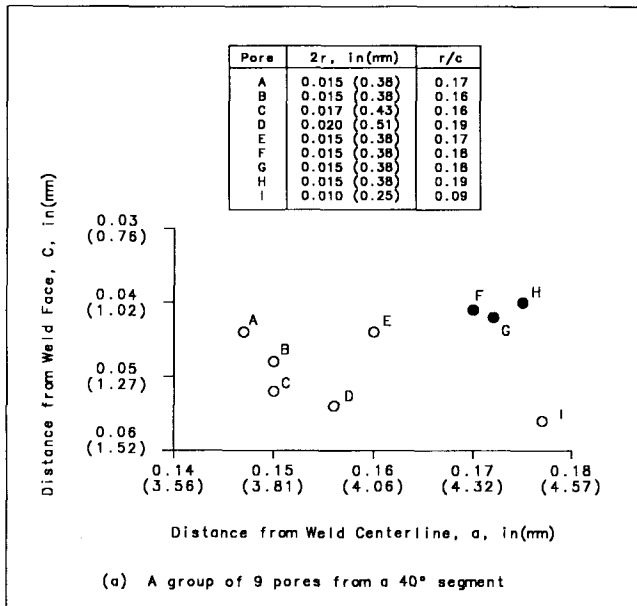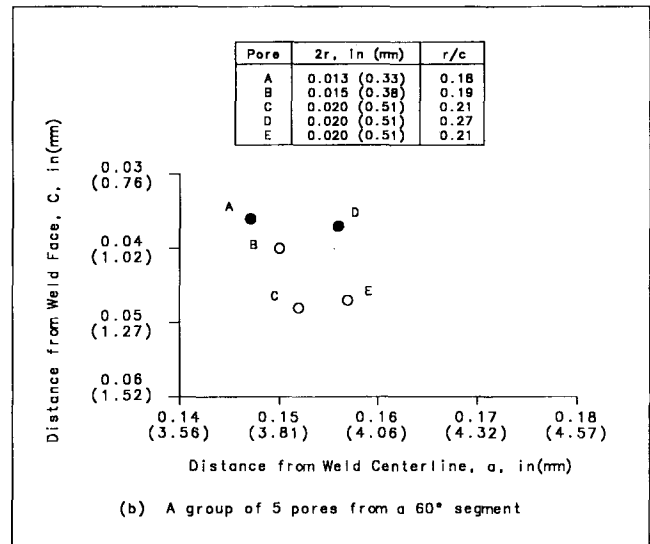
Fig. 24 Cracked (open circles) and uncracked (closed circles) pores in two locations (a) and (b) around the girth weld of S/N 33.

Table 7 Typical Auger analysis, wt%

	Element							
	S	Cl	K	C	O	Al	V	Ti
Pore surface	22.53	2.30	15.52	2.17	4.81	...	...	52.67

fusion-zone geometries; only pores from adjacent locations, having more-or-less similar fusion-zone geometries could be meaningfully compared. Within each group, uncracked pores with diameters of about 0.01 in. (~0.25 mm) and less were excluded because these tended not to crack, regardless of their position. The results of this exercise, for two such groups in S/N 33, are shown in Fig. 24. It is seen that deep pores that are farther from the weld face are more likely to crack than those shallow pores that are close to the weld face. Furthermore, this is seen to be the case, regardless of pore sizes and in spite of r/c ratios that frequently imply the exact opposite. It is clear, therefore, that pore cracking is governed by some factor other than pore size or the r/c dependent K_t.

In section 4.1, it is argued that residual stresses play a role in pore cracking. Consequently, an explanation of the results of Fig. 24, in terms of residual-stress distribution, was sought. It has been shown that, in welds, the peak residual tensile stresses occur at some distance below the weld face and that the magnitude of these stresses decreases toward the weld root and face.[32] Considering that pore cracking is governed by the magnitude of residual tensile stresses, then those pores closer to the weld face would be less likely to crack, which is indeed what Fig. 24 depicts.

It is believed, therefore, that pore cracking is governed by residual-stress distribution within the weld. In those regions where residual tensile stresses exist, the cracking tendency is modified by the K_t value of the particular pore, which is a function of pore size and depth below the surface.

4.3 Fracture Sequence and X-Ray Detectability

The tear ridges, seen converging to the pores, indicate that crack initiation occurs independently at multiple locations around a given pore. The crack ligaments thus initiated then propagate in two main directions. The first is the lateral direction around the pore (lateral spreading), with those ligaments eventually linking up with one another via the formation of tear ridges; the wavy shapes of the fracture fronts seem to support that view. The second direction is outward, away from the pore. Eventually, some of the outward propagating cracks will reach their nearest free surface. Once a free surface is breached, a wedge is created, which gives rise to a notch effect that is more severe than that of the original pore.[9] This tends to accelerate crack propagation toward the opposite free surface. Notch severity would be proportional to pore depth below the free surface that was breached first. A prediction of this model is that cracked pores close to a free surface would result in less-severe

notches and, as such, would be less likely to develop into leaks, a prediction that is supported by the results of the present work. As the crack approaches the opposite free surface, propagation is further accelerated by proximity to that surface and by the bending effects associated with the asymmetrical section.[33] The elongated and smeared appearance of zone 2 (Fig. 12) may just be a manifestation of the accelerating effects just described. When the crack ultimately reaches the opposite free surface, a leak path is formed.

Cracking is thought to begin after welding, following some incubation period. Crack initiation would be mainly governed by residual welding stresses. Propagation of existing crack ligaments would be driven by residual stresses, aided by the applied stresses resulting from the remaining fabrication operations, testing and/or the service cycles. Ultimately, when all fabrication has been completed, and when all residual stresses have been relieved by cracking, further crack propagation would be governed solely by service stresses. Initially, the crack ligaments would be fairly small and tight, making them difficult to detect by nondestructive methods, such as X-ray inspection. The problem would be further compounded by the presence of the overwrap and by the double-wall inspection technique that has to be used. The fact that the crack associated with leak site 3 in S/N 33 (Fig. 17) was not detected by X-ray inspection seems to support that view. Even after removal of the overwrap, small cracks such as that of Fig. 20(a) could not be detected by X-ray inspection.

A plausible scenario of pore cracking assumes a two-stage process. In the first stage, initiation and growth of the crack ligaments is governed mainly by residual stresses, giving rise to zone 1 quasicleavage. This being a slow process, very long times would be required for the cracks to grow to detectable sizes. It is conceivable, therefore, that the cracks would remain undetectable well after all fabrication and inspection operations have been completed. Some time after the conclusion of these operations, the vessel is placed in service, without further X-ray inspection. During that time, crack growth does not cease, and more zone 1 quasicleavage forms. In the second stage (zone 2), crack growth is governed mainly by service stresses. The long dwell periods, typical of service cycles coupled with the free-surface proximity effects, leads to fairly large crack extensions, resulting in the formation of leak paths after only a few service cycles.

4.4 Embrittlement and Pore Cracking

Current thinking seems to attribute pore cracking to some sort of local embrittlement around the pores, brought about by the constituents involved in pore formation. In the present work, some manifestation of that embrittlement was sought metallographically and by microhardness measurements. These techniques, however, did not reveal any microstructural or hardness changes that could be associated with or attributed to the presence of pores. It was suspected that embrittlement may have been caused by gases existing within the pores. However, RGA revealed that the gases, initially involved in pore formation, have diffused away from the pores into the weld metal. It was then reasoned that embrittlement may be caused by interstitials in solid solution, present in the weld metal surrounding the pores. Bulk chemical analysis, however, provided

no support to that argument. In fact, bulk analysis shows that the base metal has more oxygen and hydrogen than the weld, suggesting that, if interstitial embrittlement were the issue then it is the base metal, not the weld, that should be failing. The only significant chemical result in this work was a sulfur enrichment, detected by Auger analysis, at the pore surfaces. Sulfur, however, does not appear to be particularly embrittling to titanium.[34]

Because a direct proof of embrittlement was not possible, some indirect means were attempted. It was theorized that zone 1 quasicleavage might just be a manifestation of embrittlement that is too subtle to verify by direct means, that is, the quasicleavage is not a consequence of the fracture mechanism. This theory, however, was dismissed as invalid, because zone 1 type of quasicleavage occurs in weld failures, regardless of whether or not a pore is involved.[15] It was then rationalized that perhaps volume-to-surface-area (V/S) ratios could provide some clue as to the existence of embrittlement. In this approach, it is recognized that larger pores have larger V/S ratios. Consequently, more of the embrittling species would be available to enrich nearby regions as these species migrate out of the pores. This would cause the larger pore sites to become more embrittled than the smaller pores sites and thus be more prone to cracking. The results of the present work, however, show that that is not the case.

It appears, therefore, that the pore cracking phenomenon could not be the result of local embrittlement around the pores. Rather, pore cracking is thought to be a direct result of the general susceptibility of titanium and its alloys to SLC. This would especially be the case for welds,[26] due to their inherent lack of ductility. The problem is further aggravated by the stress-concentration effects associated with the presence of pores,[19] and by possible interstitial pickup during welding and other fabrication operations. Interstitial pickup, however, would uniformly affect the ductility of the entire weld, not just the pore sites.

4.5 Weld Ductility, Residual Stresses, and Thermal Treatments

In vessel fabrication (section 1.3), an annealing treatment at 1175 °F (635 °C) for 2 h is used after welding. One goal of this thermal treatment is to improve weld ductility and the other is to relieve residual stresses. It is felt that thermal treatment at higher temperatures for longer periods of times would be more effective in achieving these goals. One such treatment involves annealing in the 1300 to 1350 °F (704 to 732 °C) temperature range for a minimum of 4 h. Other thermal treatments, involving even higher temperature anneals, have been shown to be very effective for Ti-6Al-4V welds (see Ref 35, 36). The applicability of these thermal treatments to pressure vessels and their effects, if any, on pore cracking should be investigated. It must be recognized, however, that in order to preclude the initiation of cracks under action of residual stresses, such thermal treatments should be performed soon after welding.

4.6 SLC and Hydrogen Effects

It is an established fact that titanium and its alloys are susceptible to SLC. The SLC phenomenon, however, is not fully

understood. What is known is that the presence of certain elements tends to have an adverse effect on SLC. It has been repeatedly shown that hydrogen is one such element (see Ref 26, 37, 38). The role of hydrogen has often been explained in terms of stress-induced diffusion to crack tips (see Ref 39, 40). The fact that the effects of hydrogen on SLC have been extensively investigated appears to have led many to develop the logic that this element is the sole cause of SLC, even though the alloys they studied had very low hydrogen content bordering on the limit of detectability. This exclusive hydrogen role has been questioned.[25,26,41] Some authors[26,41] argued that hydrogen is influential, rather than causative of SLC, while others[25] suggested a role for oxygen. Interestingly, a model for stress-induced diffusion of oxygen, similar to that of hydrogen, has been proposed.[42] Furthermore, oxygen has been shown to have an adverse effect on SLC[43] and also on fatigue properties[44,45] of titanium alloys. It is believed, therefore, that the susceptibility of titanium alloys to SLC is influenced by all the interstitial elements present, not just hydrogen. Alloy condition (ST, STA, A, etc.) and microstructure are also influencing factors.[43] Susceptibility to SLC is thought to impose a basic limitation as to the use of welded titanium alloys in at least some pressure-vessel applications. As such, a reassessment of the theories concerning SLC seems warranted.

5. Conclusions

The observed weld porosity appears to be caused by gaseous products, resulting from reaction of the molten metal with surface films present on joint and filler-wire surfaces. Contributing to these films are machining oils, cleaning solutions, and similar substances used in fabrication. Pore surface appearance indicates that the gaseous products in question are either neutral or reducing in nature. Residual gas analysis, however, indicates that these gaseous products have diffused away from the pores into the weld metal.

Pore cracking initiates at the pores and then propagates to breach the free surfaces, leading to the formation of leak paths. Size is not the governing factor in pore cracking. Pore cracking occurs by dwell-time fatigue, a mechanism that involves both sustained-load and cyclic contributions, with the former being the more prominent. As such, pore cracking is essentially a sustained-load cracking (SLC) phenomenon, brought about by residual-welding stresses and the long dwell times of the service cycles. Pore cracking is not the result of local embrittlement around pores. Rather, it is a direct result of the general susceptibility of titanium alloys to SLC. The problem is further aggravated by a lack of ductility that is inherent to welds, and by the stress-concentration effects associated with pore presence.

Interstitial content of the weld as well as the final alloy condition and microstructure are thought to be influencing factors in SLC behavior. The basic susceptibility of titanium alloys to SLC is thought to be due to all the interstitial elements present, not just hydrogen.

Deep pores that are farther from the weld face are more likely to crack than those shallow pores closer to the weld face. Only the cracks associated with deep-laying large pores are more likely to develop into leaks.

References

1. D.G. Howden, *Weld. J.*, Vol 50 (No. 2), 1971, p 112
2. D.G. Howden, *Weld. J., Res. Suppl.*, Vol 61 (No. 4), 1982, p 103-S
3. I.D. Harris, "A Review of Porosity Formation and Recommendations on the Avoidance of Porosity in TIG Welding," Report 387, The Welding Institute, 1987
4. J.W. Bradley and R.B. McCauley, *Weld. J., Res. Suppl.*, Vol 43 (No. 9), 1964, p 408-S
5. A.I. Gorshkov, *Weld. Prod.*, Vol 15 (No. 7), 1968, p 41; trans. from Russian
6. R.M. Evans, "Porosity in Titanium Welds," DMIC Memorandum 194, Battelle Memorial Institute, 8 June 1964
7. D.R. Mitchell, *Weld. J., Res. Suppl.*, Vol 44 (No. 4), 1965, p 157-S
8. M.M. D'Andrea, Jr., *Weld. J., Res. Suppl.*, Vol 45 (No. 3), 1966, p 178-S
9. F.V. Lawrence, Jr., W.H. Munse, and J.D. Burk, "Effects of Porosity on the Fatigue Properties of 5083 Aluminum Alloy Weldments," Bulletin No. 206, Welding Research Council, 1975
10. "Feasibility Study for Producing Navaho Components from Titanium," Report AL-2214-3 (Air Force Contract 33-600-30902), North American Aviation, 15 Dec 1955
11. R.P. Olsen and J. Gates, *Weld. J., 37*(No. 5), May 1958, p 478
12. C. Walker, "Metallurgical Investigation of Four Experimental Ti-6Al-4V Pressure Vessels," Test No. T5-1380, Boeing Airplane Co., 7 Aug 1958
13. F. Godfrey and R. Makowski, "Research and Development of Titanium Rocket Motor Case, Vol III—Development of Welding Practice," Technical Report WAL 766.2/1-14, Pratt and Whitney Aircraft, 31 Oct 1963
14. J. Kennedy and R. Schulte, *J. Mater. Sci.*, Vol 21, 1986, p 4424
15. T.E. Collins and T. Khaled, "Investigation of Weld Pore Cracking in MPS Helium Pressurization Tank S/N 33," Report SSD92D0248, Rockwell International, Feb 1992
16. J.T. Kenny, "RCS Tank Girth Weld Flaw Investigation Report TA-1," Report No. C87376, Martin Marietta Corp., Denver, CO, Aug, 1979.
17. T. Khaled and M.R. Leifeste, "Failure Analysis of He Tank (S/N 35)," Laboratory Test Report LTR 4088-2454, Rockwell International, Feb 1993
18. S.M. Gurevich, O.K. Nazarenko, V.N. Zamkov, V.E. Lokshin, and A.D. Sheveler, *Titanium 80, Science and Technology*, H. Kimura and O. Izumi, Ed., TMS-AIME, 1980, p 2347
19. E. Tsuchida and I. Nakahara, *Bull. Jpn. Soc. Mech. Eng.*, Vol 13, 1970, p 499
20. "Low Cycle Fatigue Design Data on Materials in Multi-Axial Stress Field," Report TDR-63-4094, Air Force Materials Laboratory, Nov 1963

21. "Biaxial Strength Characteristics of Selected Alloys in a Cryogenic Environment," Report 2-53420/6R-2279, LTV Aerospace Corp., 6 May 1966

22. E. Litwinski, R. Mines, D. Wittman, and T. Khaled, "Fractography and Fracture of Ti-6Al-4V; Interim Progress Report," Laboratory Test Report LTR 5986-2450, Rockwell International, 1 Dec 1992

23. E.H. Rennhak and W.B. Burger, Titanium 80, Science and Technology, H. Kimura and O. Izumi, Ed., TMS-AIME, 1980, p 419

24. D.N. Williams, Metall. Trans., Vol 5 (No. 11), 1974, p 2351

25. G.R. Yoder, C.A. Griffis, and T.W. Crooker, J. Eng. Mater. Technol. (Trans. ASME), 96(No. 10), Oct 1974, p 268

26. D.A. Meyn, Metall. Trans. A, Vol 5 (No. 11), 1974, p 2405

27. D. Eylon, T.L. Bartel, and M.R. Rosenblum, Metall. Trans. A, Vol 11 (No. 8), 1980, p 1361

28. D. Eylon and M.R. Rosenblum, Metall. Trans. A, Vol 13 (No. 2), 1982, p 322

29. J.E. Hack and G.R. Leverant, Metall. Trans. A, Vol 13 (No. 10), 1982, p 1729

30. W.J. Evans and C.R. Gostelow, Metall. Trans. A, Vol 10 (No. 12), 1979, p 1837

31. J.C. Chestnut and N.E. Paton, Titanium 80, Science and Technology, H. Kimura and O. Izumi, Ed., TMS-AIME, 1980, p 1855

32. R.H. Leggatt, Residual Stresses at Circumferential Welds in Pipes, Weld. Inst. Res. Bull., June 1982, p 181

33. R.M. Ehret, "Fracture Control Methods for Space Vehicles, Vol II—Assessment of Fracture Mechanics Technology for Space Shuttle Applications," Report CR-134597, NASA, 1974

34. L.W. Berger, D.N. Williams, and R.I. Jaffee, Trans. ASM, Vol 49, 1957, p 300

35. K. Borggreen and I. Wilson, Weld. J., Res. Suppl., Vol 61 (No. 1), 1982, p 1-S

36. G. Thomas, V. Ramachandra, M.J. Nair, K.V. Ngarajan, and R. Vasudevan, Weld. J., Res. Suppl., Vol 71 (No. 1), 1992, p 15-S

37. R.R. Boyer and W.F. Spurr, Metall. Trans. A, Vol 9 (No. 1), 1978, p 23

38. N.R. Moody and W.W. Gerberich, Metall. Trans. A, Vol 11 (No. 6), 1980, p 973

39. H. Margolin, Metall. Trans. A, Vol 7 (No. 8), 1976, p 1233

40. W.J. Pardee and N.E. Paton, Metall. Trans. A, Vol 11 (No. 8), 1980, p 1391

41. D.A. Meyn, "Fractography—Microscopic Cracking Processes," STP 600, ASTM, 1976, p 75

42. Y.A. Bertin, J.L Gacougnole, J. Parisot, J. de Fouquet, and D. Beshers, Titanium 80, Science and Technology, H. Kimura and O. Izumi, Ed., TMS-AIME, 1980, p 529

43. A. Tobin, "Effect of Hydrogen, Oxygen and Microstructure on Sustained Load Subcritical Crack Growth," Research Memorandum RM-720J, Grumman Aerospace Corp., 1981

44. A.W. Thompson, J.D. Frandsen, and J.C. Williams, Metal Science, Vol 9, The Metals Society, 1975, p 46

45. G.T. Gray III, G. Luetjering, and J.C. Williams, Metall. Trans. A, Vol 21 (No. 1), 1990, p 95